



DESY SUMMER STUDENT PROGRAMME 2012

Hamburg, July, 17th - September, 6th

**Normalized Differential Top Quark Pair Production
Cross Sections in the e/μ + jets Decay Channels**

**Single Top Quark Quantities and
Lepton Charge Asymmetries**

Valeria Botta

Università degli Studi di Perugia, Italy

supervised by

Thomas Hermanns

Universität Hamburg, Germany

Abstract

Two investigations in the framework of semileptonic (electron and muon) top quark pair analysis have been performed based on 2011 LHC data: a comparison of top and antitop quarks regarding their behaviour with respect to transverse momentum and rapidity, and a comparison of positively and negatively charged leptons with respect to their dependence on pseudorapidity. All distributions for both top and antitop quarks as well as for positively and negatively charged leptons agree very well within uncertainties. This implies that for charge asymmetries being predicted by the Standard Model values not significantly deviating from zero can be determined, too. The present analysis is not sensitive to measure them from distributions directly depending on transverse momentum, rapidity, or pseudorapidity.

Contents

1	Introduction	3
1.1	The Large Hadron Collider	3
1.2	CMS Experiment	4
1.2.1	Reference Frame and Kinematic Variables	6
1.3	Top Quark Pair Production at the LHC	7
1.3.1	Production processes	7
1.3.2	Decay channels	7
1.3.3	Signature, Background and Event Selection for the Semileptonic Final State	8
1.3.4	Event Reconstruction	10
2	Charge Asymmetry	11
2.1	Differential and Integrated Asymmetry	11
2.2	Charge Asymmetry of Top Quark Pairs	11
3	Data Analysis	13
3.1	Definition of Cross Sections	13
3.2	Top and Antitop Quark Distributions	14
3.2.1	Raw Asymmetries	14
3.2.2	Cross Section Asymmetries	18
3.3	Charged Lepton Distributions	21
3.3.1	Raw asymmetry	21
3.3.2	Cross Section Asymmetry	23
3.3.3	Integrated Asymmetry	25
4	Conclusions	26
5	Acknowledgments	27
6	References	27

1 Introduction

1.1 The Large Hadron Collider

The Large Hadron Collider LHC is a particle accelerator operated at CERN near Geneva in Switzerland for frontier research in fundamental high energy physics. It is installed in the 26.7 km long tunnel, which formerly hosted the Large Electron-Positron collider (LEP). The LHC has been designed to collide two proton beams containing bunches of about 10^{11} protons every 25 ns at a center of mass energy $\sqrt{s} = 14 \text{ TeV}$.

In 2011, the year for which the following studies have been performed, it was operated at 7 TeV with collisions every 50 ns.

The number of interactions, at which a certain physics process takes place, is measured by the luminosity that is the proportionality factor between the number of events per second $\frac{dR}{dt}$ and the cross section of this process:

$$\frac{dR}{dt} = \mathcal{L} \sigma$$

For an intersecting storage ring collider the luminosity is given as:

$$\mathcal{L} = \frac{f n N_1 N_2}{A} \quad (1)$$

where f is the revolution frequency of the proton beam, n is the number of bunches in one beam in the storage ring, N_i is the number of particles in each bunch, and A is the beam transverse cross section. The luminosity has the dimension of $[m^{-2}s^{-1}]$ and it is usually measured in $[fb^{-1}s^{-1}]$.

The integrated luminosity is defined as the integral of (1) over time:

$$L = \int \mathcal{L} dt$$

In 2011 more than 5 fb^{-1} at $\sqrt{s} = 7 \text{ TeV}$ have been recorded. Figure 1 shows the evolution of the integrated luminosity over time.

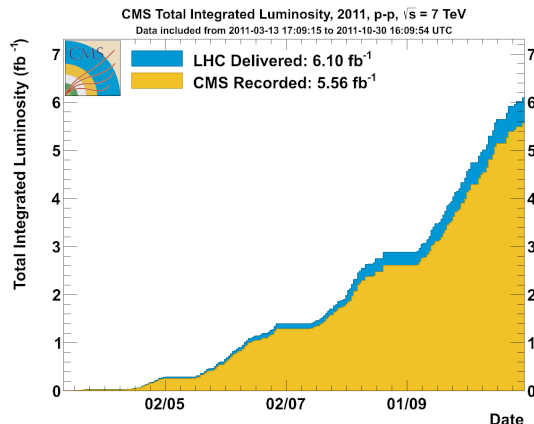


Figure 1: Evolution of the integrated luminosity delivered from LHC and recorded by CMS over time in 2011 [2].

1.2 CMS Experiment

The Compact Muon Solenoid (CMS) experiment is one of two large general purpose particle physics detectors at the LHC. The main aims of the experiment are to explore physics at the TeV energy scale, to search for the Higgs boson, and to look for evidence of physics beyond the standard model.

The CMS main component is a superconducting solenoid providing an axial magnetic field of 3.8 T, that is needed to bend high energetic charged particles.

The CMS detector is located around the beam line on the fifth interaction point of the LHC ring. It has a cylindrical symmetric structure with respect to the beam axis. In order to identify particles produced by the pp collisions and to perform kinematic measurements the detector is made up by different complementary parts.

Immediately around the interaction point the inner silicon tracker serves to identify the tracks of individual particles and match them to the collision vertices from which they originated. It consists of a silicon pixel and a silicon strip detector. The curvature of charged particle tracks in the magnetic field allows for the measurement of their charge and momentum.

The calorimeter surrounds the tracker and allows for destructive measurements of the particle energy. It consists of two parts.

The Electromagnetic Calorimeter (ECAL) is designed to measure with high accuracy the energies of electrons and photons. It is constructed from crystals of lead tungstate, an extremely dense but optically clear material, ideal for stopping high energy particles.

The Hadronic Calorimeter (HCAL) serves for measuring the energy of hadrons produced in each event.

The outer part of the detector is the muon detector, lying outside the superconducting magnet, and allowing for muon identification together with momenta

measurements. The whole detector has to be as near to hermetic around the interaction region as possible to allow events with missing energy to be identified. Combining information from all detector components, it is possible to efficiently identify particles and measure their energy and momenta.

A layout and a partial cross section of the CMS detector can be seen in Figures 2 and 3 [3].

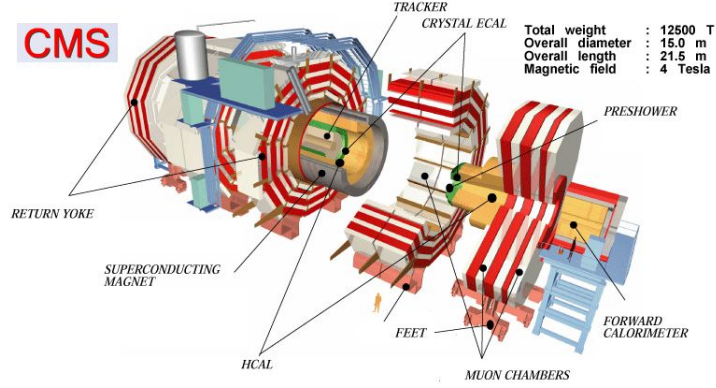


Figure 2: The CMS Detector.

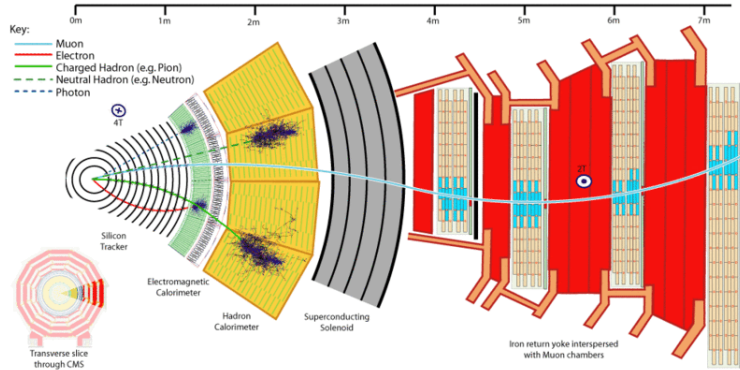


Figure 3: Particle identification by signals in different CMS subdetectors.

1.2.1 Reference Frame and Kinematic Variables

The reference frame used to describe the CMS detector and the recorded events from collisions has its origin in the geometrical center of the solenoid. Two different global coordinates are used:

- Cartesian Coordinate System: the x axis unit vector \hat{i} is oriented towards the center of the LHC, the y axis unit vector \hat{j} upwards, perpendicular to the LHC plane, and the z axis unit vector \hat{k} points in counterclockwise direction along the beam line completing a right-handed frame.
- Polar Coordinate System: the particle directions are defined with an azimuthal angle $\phi = \arctan \frac{y}{x}$ and a polar angle $\theta = \arctan \frac{r_{\perp}}{z}$, with r_{\perp} being the radius in the xy plane.

The kinematic variables used in this analysis are

- Transverse Momentum p_T :

$$p_T = p \sin \theta$$

This is the component of the particle momentum in the plane perpendicular to the beam direction.

- Rapidity y

$$y = \frac{1}{2} \ln \frac{E + p_z}{E - p_z}$$

with E being the energy and p_z the longitudinal momentum of a particle.

- Pseudorapidity η

$$\eta = -\ln \left(\tan \frac{\theta}{2} \right)$$

The pseudo-rapidity is an approximation of the rapidity for particles with mass $m \ll E, p_z$. For massless particles, rapidity and pseudo-rapidity are identical.

- Missing Transverse Energy E_T^{miss}

Due to momentum conservation, as protons collide collinearly along the z direction, the vectorial sum of p_T for the final state particles is expected to be zero. Whenever this condition is not satisfied, the missing transverse energy is a hint for the presence of one or more particles escaping from the detector without being recognized, e.g. neutrinos.

1.3 Top Quark Pair Production at the LHC

The LHC is a factory for the production of top quarks with about 850 000 top quarks being produced in 2011.

Precision measurements of top quark quantities can both provide further test for the validity of the Standard Model or hints for evidence of new physics beyond the Standard Model. Due to its high mass ($m_t \approx 172 \text{ GeV}$), the top quark lifetime $\tau_t \approx 0.5 \cdot 10^{-24} \text{ s}$ is much smaller than the typical time of $3 \cdot 10^{-24} \text{ s}$ needed to create bound top-antitop quark states. As a consequence, the top quark decays before it can hadronize and therefore offers the opportunity to study the properties of a bare quark, enabling options for precision measurements like differential cross sections measurements.

1.3.1 Production processes

At the LHC energy scale, the main process for top quark pair ($t\bar{t}$) production is gluon-gluon fusion accompanied by quark-antiquark annihilation. The dedicated Feynman diagrams at Born-level are shown in Figure 4.

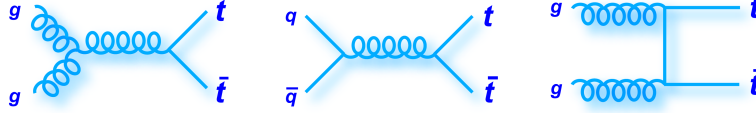


Figure 4: $t\bar{t}$ pair production diagrams.

1.3.2 Decay channels

The top quark decays via the electroweak interaction mediated by a charged W boson

$$t \rightarrow W + b$$

The b quark then constitutes a hadronic jet in the final state, while the W boson decays further in a hadronic or leptonic decay mode:

$$W \rightarrow qq'$$

$$W \rightarrow l\nu_l$$

Due to the conservation of the electromagnetic charge, top and antitop quarks decay as follows:

$$t \rightarrow W^+ + b$$

$$\bar{t} \rightarrow W^- + \bar{b}$$

The charge of the lepton originating from a leptonically decaying W boson is positive if it comes from a t quark and negative if it comes from a \bar{t} quark. Concerning a $t\bar{t}$ pair, there are three different final states, depending on the number of leptons:

- two b-jets + four light jets (fully hadronic decay): both W bosons decay hadronically
- one lepton + one neutrino + two light jets + two b-jets (semileptonic decay): one W boson decays leptonically, the second one hadronically
- two leptons + two neutrinos + two b-jets (dileptonic decay): both W bosons decay leptonically

Figure 5 shows the branching ratio for the three channels.

Top Pair Decay Channels						
$c\bar{s}$	electron+jets	muon+jets	tau+jets	all-hadronic		
$u\bar{d}$						
τ^-	et	$\mu\tau$	$\tau\tau$	tau+jets		
μ^-	e μ	$\mu\mu$	$\mu\tau$	muon+jets		
e^-	e e	e μ	et	electron+jets		
W decay	e^+	μ^+	τ^+	$u\bar{d}$	$c\bar{s}$	

Figure 5: Branching ratios of the various $t\bar{t}$ decay channels.

1.3.3 Signature, Background and Event Selection for the Semileptonic Final State

This analysis focuses on the semileptonic decay channel (Figure 6)

$$t\bar{t} \rightarrow W^+W^-b\bar{b} \rightarrow l^{(\pm)}\nu_l qq'$$

where the final state is characterized by one lepton (either μ or e in this analysis), two b-jets, two light jets and missing transverse energy induced by the neutrino.

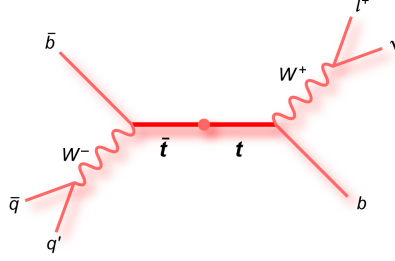


Figure 6: Feynman diagram for a semileptonic $t\bar{t}$ decay.

There are several background processes that mimic similar final states, e.g:

- $W + jets \rightarrow 1l + jets + \nu$
- single top quark events, mainly associated to the production of tW :
 $tW \rightarrow 1l + 1b\text{ jet} + 2\text{ jets} + \nu$
- $Z + jets \rightarrow 2l + jets$
- diboson events: $WW / ZZ / WZ$ decaying into leptons, ν , jets
- $t\bar{t} \rightarrow b\text{ jet} + 2\text{ jets} + \tau + \nu$ where $\tau \rightarrow \mu(or e) + \nu$
- QCD multijet events: due to the high number of pure QCD interactions, it may happen that one of the jets producing a signal in the ECAL only is reconstructed as an electron.

In order to select events and suppress the background the final state requires:

- four high p_T jets, where at least two of them are identified as b-jets using a combined secondary vertex algorithm. The jets are required to lie within a kinematic range of $p_T > 30\text{ GeV}$ and $|\eta| < 2.4$;
- exactly one isolated, high p_T lepton, with a transverse momentum $p_T > 30\text{ GeV}$ and $|\eta| < 2.1$. Electrons in the η range of 1.4442 to 1.5660, corresponding to the transition region of the barrel and end-cap calorimeter, are not taken into account.

Finally, the event composition after the full event selection comprises more than 90% $t\bar{t}$ applying the above mentioned criteria. The largest remaining background sample are single top events with about 4%. All other background events like vector-boson production or QCD multijet events are expected to accumulate to less than 5%. Without the requirement of two jets identified as b-jets the production of W bosons with additional jets is the most relevant background (30 to 35%). QCD multijet events are efficiently suppressed already by requiring an isolated, high-energetic lepton.

1.3.4 Event Reconstruction

To obtain differential measurements in quantities of the top quark itself, a reconstruction of the event topology is needed: the measured leptons and jets need to be correctly assigned to the underlying particles from the top quark pair decay.

The measured four momentum vectors of the selected lepton and jets are given as initial values to the kinematic fit. The initial neutrino four momentum vector is constructed from the missing transverse energy under the assumption of $p_z = 0$.

The kinematic fit varies now the kinematics of the objects (lepton, neutrino and jets) according to the detector resolution to fulfill certain constraints, assuming the semileptonic event hypothesis. For this analysis three constraints are used: the invariant mass of lepton and neutrino as well as two light quarks on the other hand are required to reproduce the W-boson mass $m_W = 80.4 \text{ GeV}$. Furthermore, the reconstructed top mass of the leptonic and hadronic decay branch are required to be equal.

2 Charge Asymmetry

2.1 Differential and Integrated Asymmetry

The *differential asymmetry* between two distributions $f_1(x), f_2(x)$ as a function of the variable x can be defined as

$$a(x) = \frac{f_1(x) - f_2(x)}{f_1(x) + f_2(x)} \quad (2)$$

In order to quantify the asymmetry one can associate a numerical value obtained by

$$A = \frac{\int_a^b |f_1(x) - f_2(x)| dx}{\int_a^b f_1(x) + f_2(x) dx} \quad (3)$$

which is referred to as *integrated asymmetry*. Potential values for A lie in the interval $[0; +1]$.

2.2 Charge Asymmetry of Top Quark Pairs

The charge asymmetry is the difference in angular distributions between top and antitop quarks.

In the standard model a small charge asymmetry in $t\bar{t}$ production through quark-antiquark annihilation appears in QCD calculations at next-to-leading order (Figure 7); however, the only production channel contributing to the asymmetry is the $q\bar{q}$ annihilation, as the gg diagram is totally symmetric. Due to this reason, the effect at the LHC is expected to be at the percent level only due to the non-dominant production of top quark pairs via $q\bar{q}$ annihilation.

Furthermore, the interference effects correlate the direction of motion of the incoming quarks and antiquarks with the top and antitop quarks, respectively. Owing to the symmetric initial state of proton-proton collisions at the LHC, the charge asymmetry does not manifest itself as a forward-backward asymmetry; the rapidity distributions of top and antitop quarks are symmetrical around $y = 0$. However, since the quarks in the initial state are mainly valence quarks, while the antiquarks are always sea quarks, the larger average momentum fraction of quarks (Figure 8, left) leads to an excess of top quarks produced in the forward directions, while antitop quarks are produced more centrally (Figure 8, right). The rapidity distribution of top quarks in the SM is therefore broader than that of the antitop quarks.

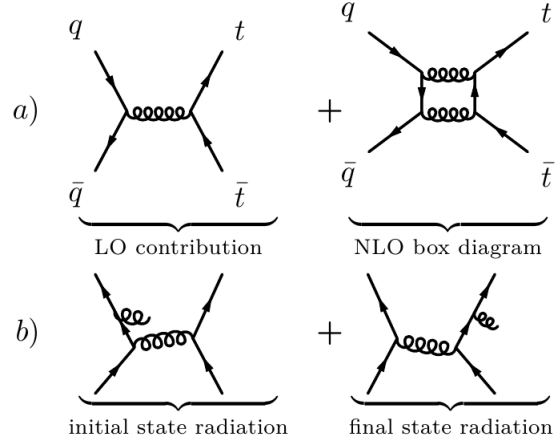


Figure 7: Interference terms contributing to the charge asymmetry.

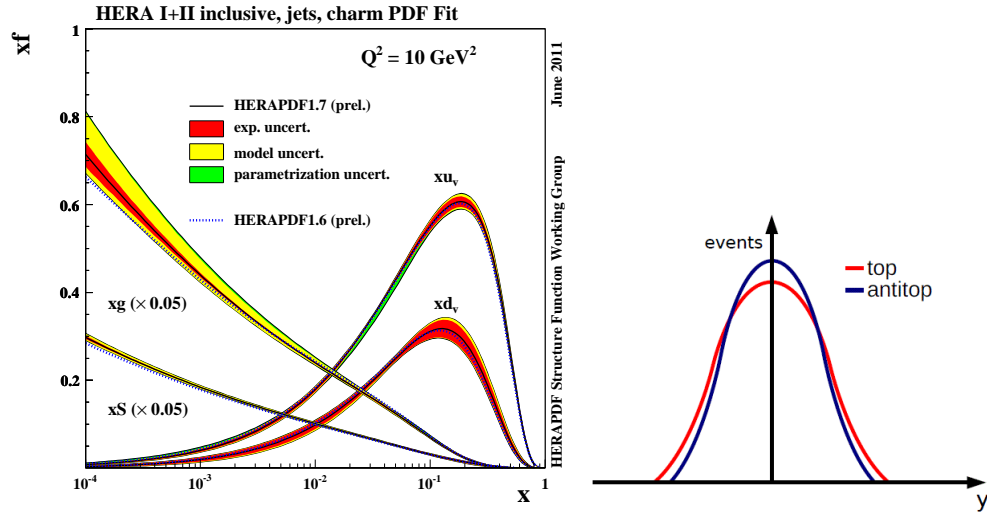


Figure 8: Parton Distribution Functions for quarks, antiquarks and gluons measured by HERA Collaboration [4] (left) and their schematic effect on top and antitop rapidity distributions (right).

3 Data Analysis

This analysis is based on both simulated and recorded data samples containing semileptonic decaying $t\bar{t}$ events from pp collisions at centre of mass energy of 7TeV . They have been analyzed for differential charge asymmetries in kinematic distributions for top and antitop quarks as well as for positively and negatively charged leptons.

The analysis is performed in two steps. First of all the *raw* asymmetry is shown. It is obtained considering the number of events in simulated samples, both for generated and reconstructed distributions.

Then, the same analysis is performed for normalized differential cross sections. They are obtained from data recorded by the CMS detector in 2011, corresponding to an integrated luminosity of 5 fb^{-1} .

3.1 Definition of Cross Sections

Experimentally, an inclusive cross section for a certain physics process is defined as

$$\sigma = \frac{N}{L A \varepsilon BR} \quad (4)$$

where N is the number of events after background subtraction, L is the integrated luminosity; the detector acceptance A, the selection efficiency ε , and the branching ratio BR are correction factors.

The differential cross sections as a function of the variable X are derived in the same way as the inclusive one, but separately for each bin in X and normalized to the bin width ΔBin_i :

$$\frac{d\sigma}{dX_i} = \frac{dN_i}{L \varepsilon_i A_i \Delta Bin_i BR} \quad (5)$$

As this is a differential quantity it has to be corrected for migration effects because there is a certain probability that an event generated in bin i is reconstructed in bin $j \neq i$. The vector \vec{t} containing the number of events generated in each bin is related to the vector \vec{m} of reconstructed events through a *response matrix* A:

$$\vec{m} = A \vec{t} \quad (6)$$

In order to obtain the correct number of events for a given bin, Eq. (6) must be inverted to evaluate the differential cross section. This operation is usually referred to as “unfolding”:

$$\frac{d\sigma}{dX_i} = \frac{\sum_j dN_j \times A_{ij}^{-1}}{L \varepsilon_i A_i \Delta Bin_i BR} \quad (7)$$

The normalized differential cross section is given by

$$\frac{1}{\sigma} \frac{d\sigma}{dX_i} = \frac{\sum_j dN_i \times A_{ij}^{-1}}{N \varepsilon_i A_i \Delta Bin_i} A \varepsilon \quad (8)$$

It is independent of L and BR . Furthermore, a general feature is that bin-independent correction factors and uncertainties cancel out.

3.2 Top and Antitop Quark Distributions

Due to the detector acceptance, the range available for the top quark rapidity is limited to $|y| < 2.5$. As top and antitop quark angular distributions are expected to be slightly different, it might be possible to observe an asymmetry rising from the wider distribution of the top quark in comparison to the antitop quark in the central rapidity region. Nevertheless, the effect is expected to be very small and this analysis has not been optimized for this measurement.

Concerning the scope of this work, the main interest in comparing top and antitop quark distributions is therefore to understand if both particles reveal similar shapes in differential cross sections in transverse momentum and rapidity distributions, neglecting for the moment the very small correction due to the charge asymmetry.

3.2.1 Raw Asymmetries

The following distributions are obtained by counting the number of top (top “Plus”) and antitop (top “Minus”) quarks as a function of their transverse momentum and rapidity. The error bars in the raw distributions only account for the statistical uncertainty, which is calculated as the square root of the bin content. Figure 9 shows the p_T (top) and y (bottom) distributions of the reconstructed top and antitop quarks. Figure 10 shows the same distributions for the generated events. For all bins the distributions of top and antitop quarks agree within uncertainties.

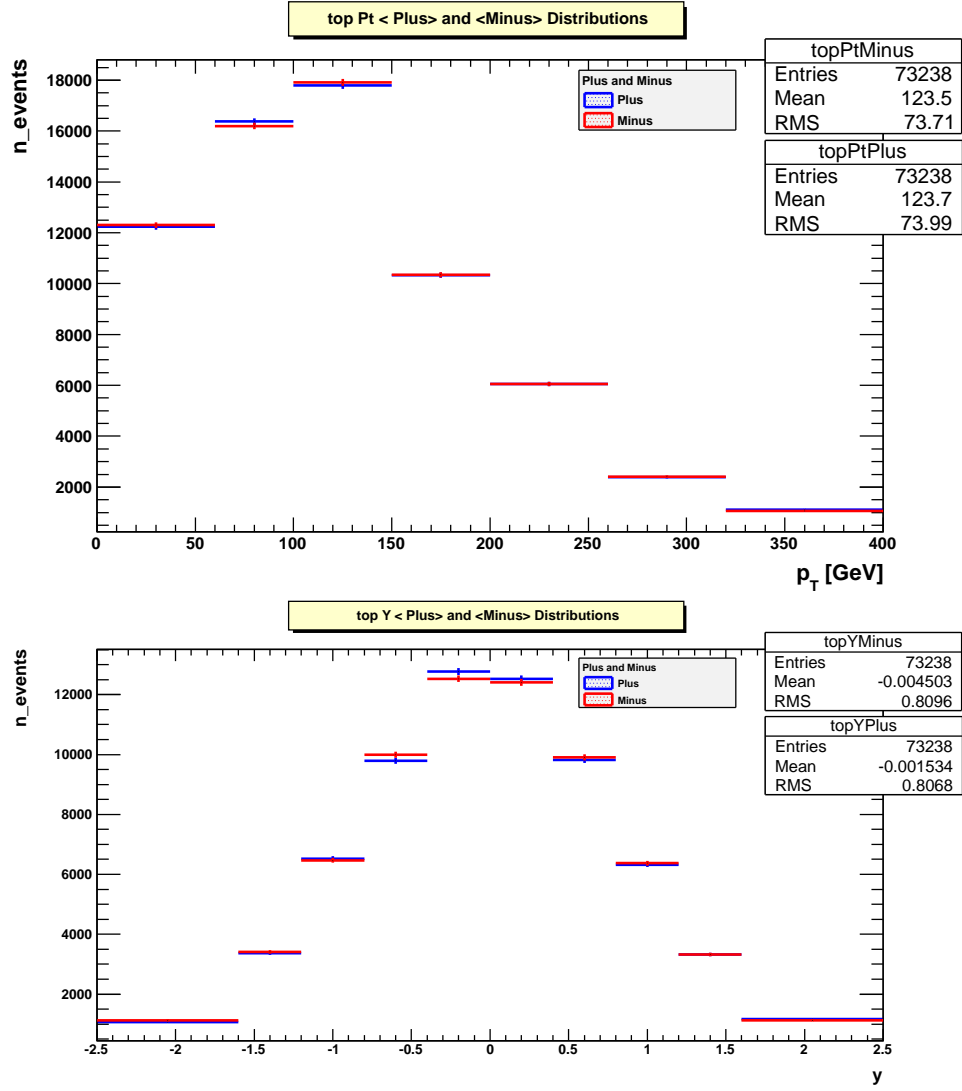


Figure 9: Raw distributions of reconstructed top and antitop quarks in transverse momentum p_T (top) and rapidity y (bottom).

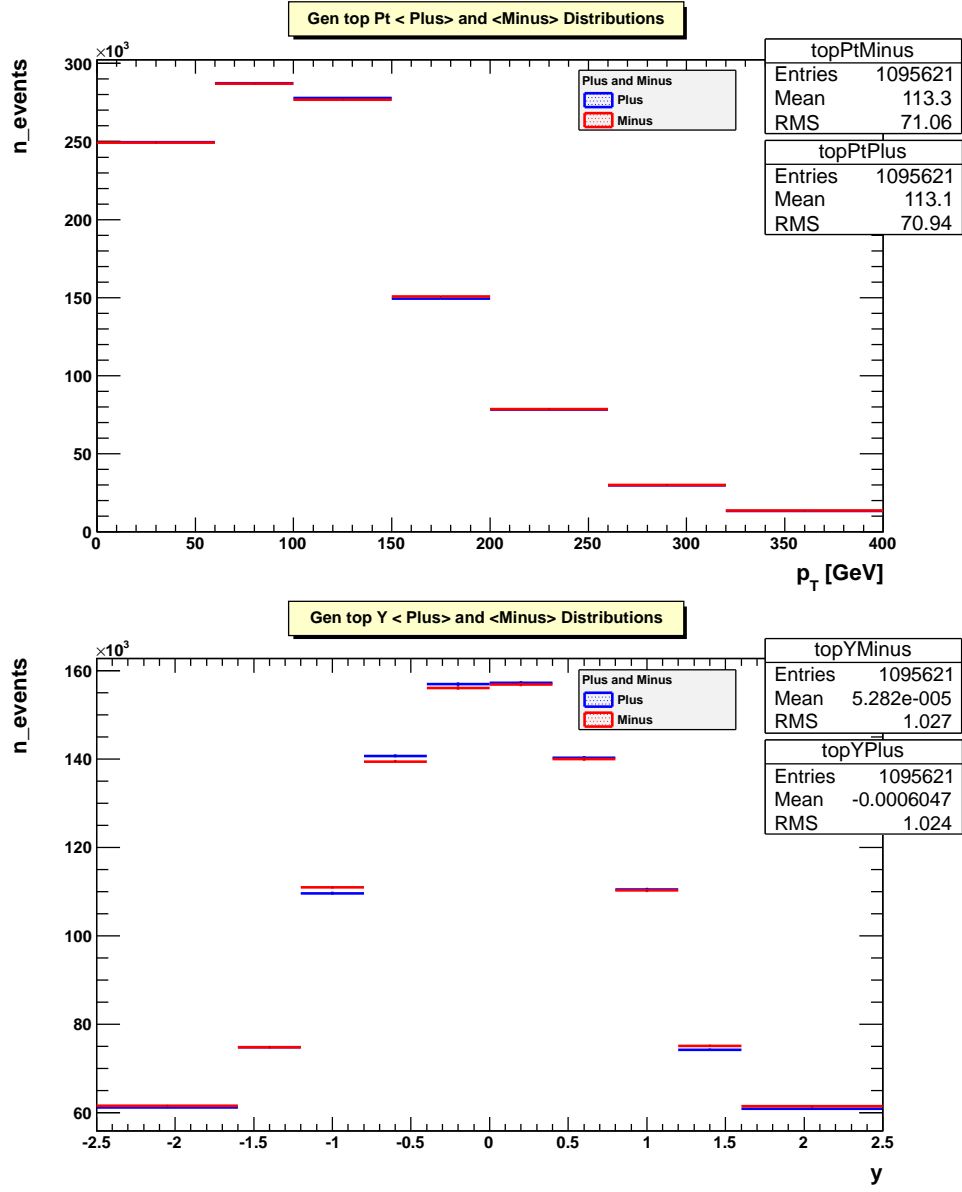


Figure 10: Raw distributions of generated top and antitop quarks in transverse momentum p_T (top) and rapidity y (bottom).

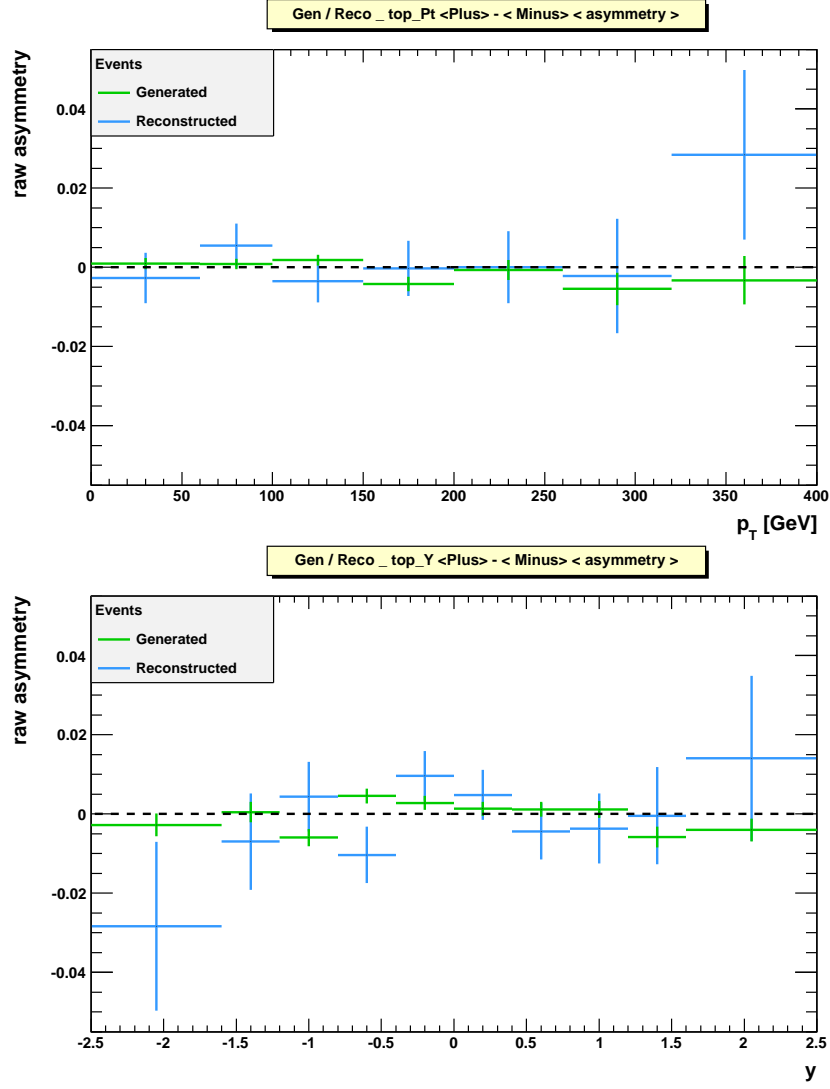


Figure 11: Differential raw asymmetries of generated and reconstructed top and antitop quarks in transverse momentum p_T (top) and rapidity y (bottom).

3.2.2 Cross Section Asymmetries

The following distributions are obtained plotting the normalized differential cross section as a function of transverse momentum (Figure 12, top) and rapidity (Figure 12, bottom) for top and antitop quarks. For all bins top and antitop quark distributions agree within uncertainties. The error bars account for both statistical and systematic uncertainties.

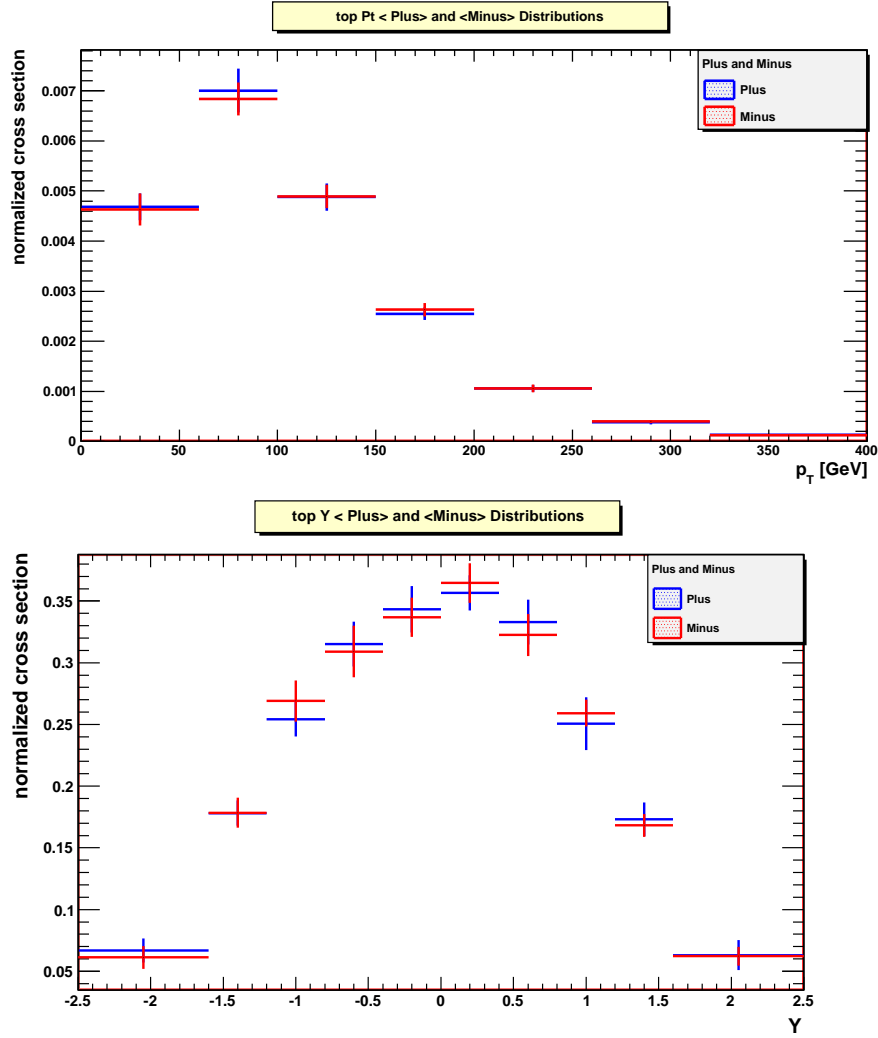


Figure 12: Normalized differential cross sections of top and antitop quarks in transverse momentum p_T (top) and rapidity y (bottom).

The differential asymmetry illustrated in Figure 13 for p_T (top) and y (bottom) is given by:

$$a(x) = \frac{\frac{1}{\sigma} \frac{d\sigma}{dx_t} - \frac{1}{\sigma} \frac{d\sigma}{dx_{\bar{t}}}}{\frac{1}{\sigma} \frac{d\sigma}{dx_t} + \frac{1}{\sigma} \frac{d\sigma}{dx_{\bar{t}}}} \quad (9)$$

Both measured differential asymmetries are flat around zero within uncertainties.

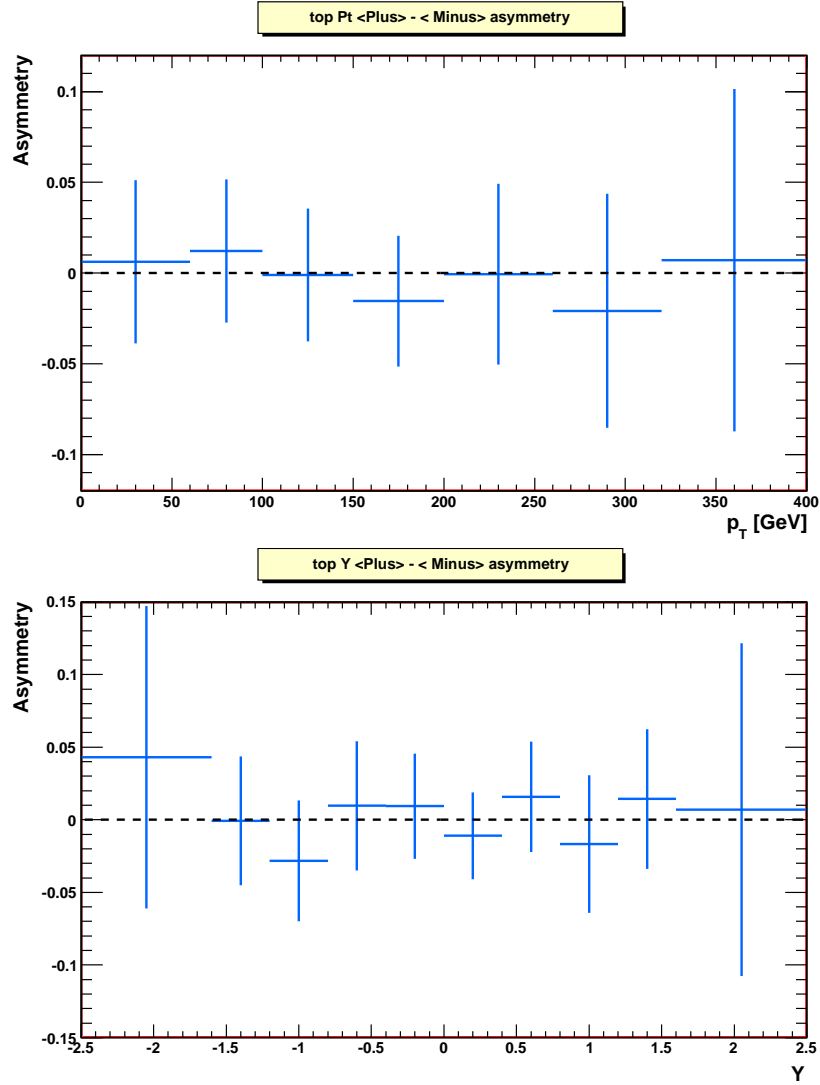


Figure 13: Normalized differential cross sections asymmetry of top and antitop quarks in transverse momentum p_T (top) and rapidity y (bottom).

Moreover, Table 1 summarizes the integrated asymmetries measurements for the top and antitop quark quantities. The measured values are mostly below 1%. The difference between reconstructed and generated level serve as a cross check to show any detector effects that can occur, leading to artificially induced effects. They are both compatible within statistical uncertainties. Concerning cross sections, the integrated asymmetry is not significantly deviating from zero.

Given this experimental setup, neither the raw distributions and asymmetries, nor the direct comparison of the differential cross section as well as the related differential and integrated asymmetries suggest that top and antitop quark behave differently in tranverse momentum or rapidity.

Table 1: Integrated charge asymmetries for top and antitop quark quantities. The raw asymmetry is obtained from a simulated data sample both for generated and reconstructed events. The cross section asymmetry is measured from the 2011 CMS data set. The uncertainties for the raw asymmetries comprise the statistics only, while the ones for the cross sections contain the statistical and systematic uncertainties.

t, \bar{t}	Raw asymmetry		Cross section asymmetry	
	Reco Level	Gen Level		
p_T	0.51 ± 0.31	0.21 ± 0.07	0.77 ± 1.91	(%)
y	0.74 ± 0.28	0.33 ± 0.07	1.48 ± 1.53	(%)

3.3 Charged Lepton Distributions

In principle, the charge asymmetry in the top-antitop rapidity distributions should lead to an asymmetry in the pseudo-rapidity distributions of the charged leptons in the final state as well: due to electromagnetic charge conservation, the leptons originating from an antitop quark are always negatively charged, and leptons coming from top quarks carry positive charge. The lepton quantities have the advantage that they can be measured with high resolution and their reconstruction does not imply combinatorial algorithms as for top quarks.

The second part of this analysis is meant as a feasibility study for the measurement of this lepton charge asymmetry in pseudorapidity distributions:

$$a(\eta) = \frac{N_+(\eta) - N_-(\eta)}{N_+(\eta) + N_-(\eta)} \quad (10)$$

where $N_+(N_-)$ refers to positively (negatively) charged leptons.

Similarly to the top quantities analysis previously performed, the asymmetry is studied in distributions of number of events and in differential cross sections. The effect is then quantified by the integrated asymmetry value.

3.3.1 Raw asymmetry

The distributions shown in Figure 14 and 15 contain the number of positively and negatively charged leptons as a function of their pseudorapidity both for reconstructed and generated events, respectively. The uncertainties comprise the statistics only.

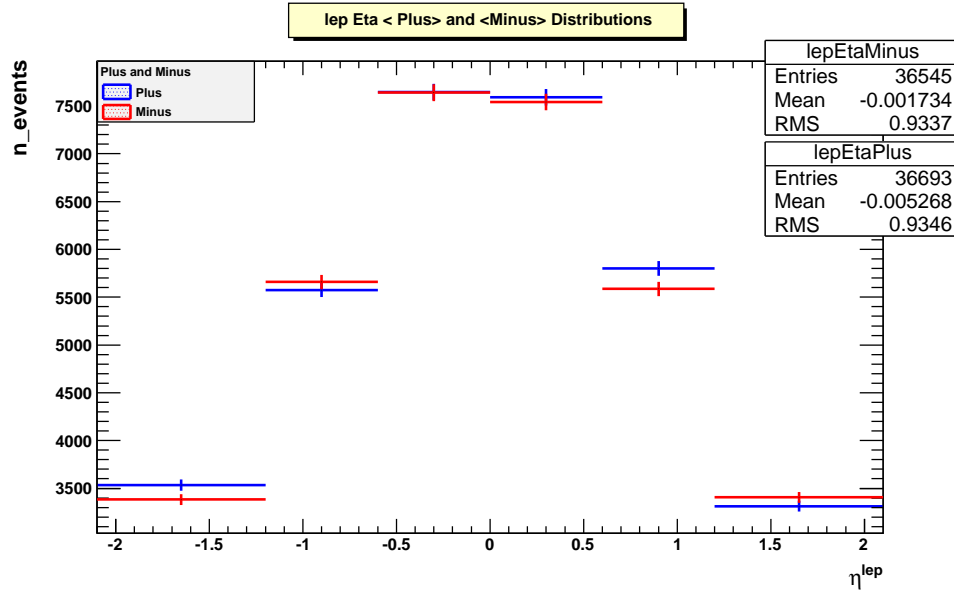


Figure 14: Raw reconstructed distribution of positively and negatively charged leptons as a function of pseudorapidity.

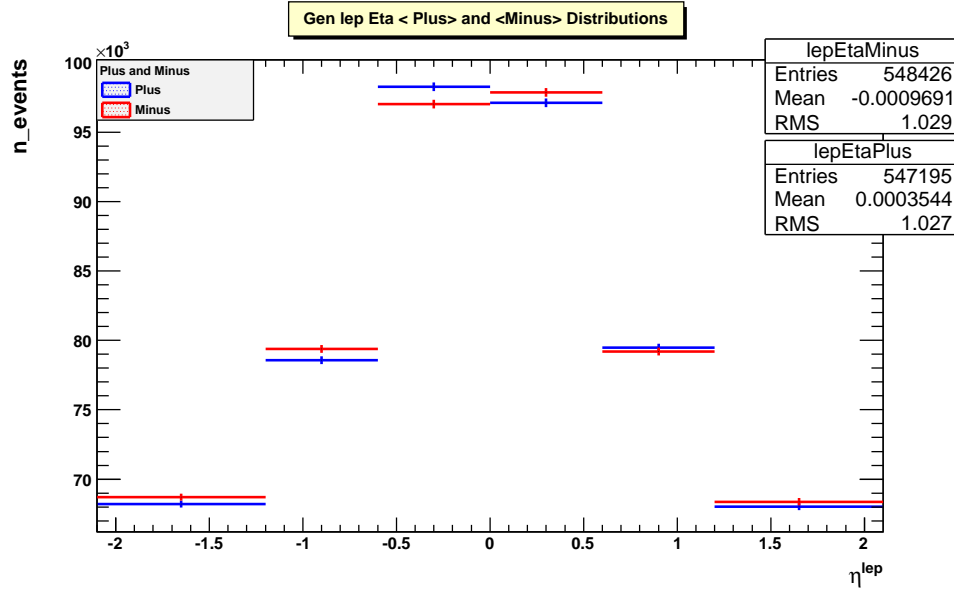


Figure 15: Raw generated distribution of positively and negatively charged leptons as a function of pseudorapidity.

A comparison of the differential lepton charge asymmetries for generated and reconstructed events is shown in Figure 16. As for the top quantities, the distributions for both generated and reconstructed events do not show any trend indicating a significant asymmetry.

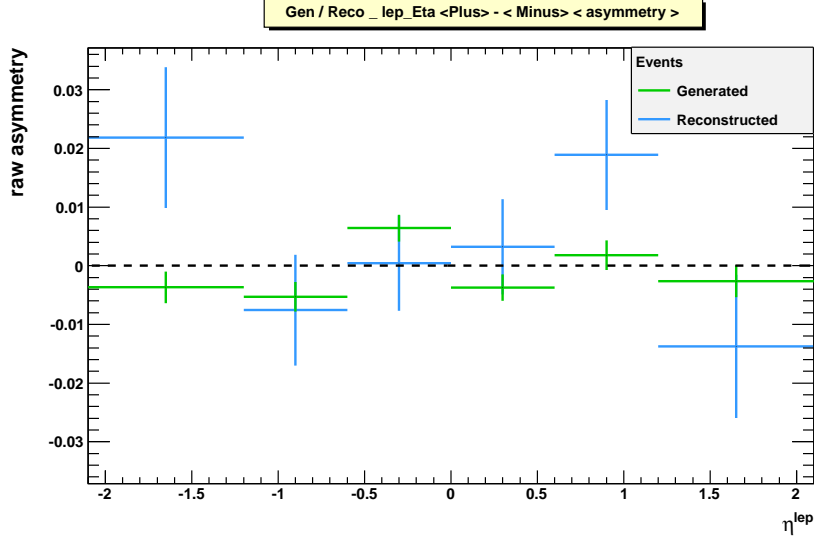


Figure 16: Raw asymmetry for reconstructed and generated charged leptons as a function of pseudorapidity.

3.3.2 Cross Section Asymmetry

The distribution in Figure 17 is obtained by plotting normalized differential cross section as a function of pseudorapidity for positively and negatively charged electrons or muons. The error bars account for both statistical and systematical uncertainties.

The differential asymmetry revealed in Figure 18 is computed by:

$$a(\eta) = \frac{\frac{1}{\sigma} \frac{d\sigma}{d\eta_+} - \frac{1}{\sigma} \frac{d\sigma}{d\eta_-}}{\frac{1}{\sigma} \frac{d\sigma}{d\eta_+} + \frac{1}{\sigma} \frac{d\sigma}{d\eta_-}} \quad (11)$$

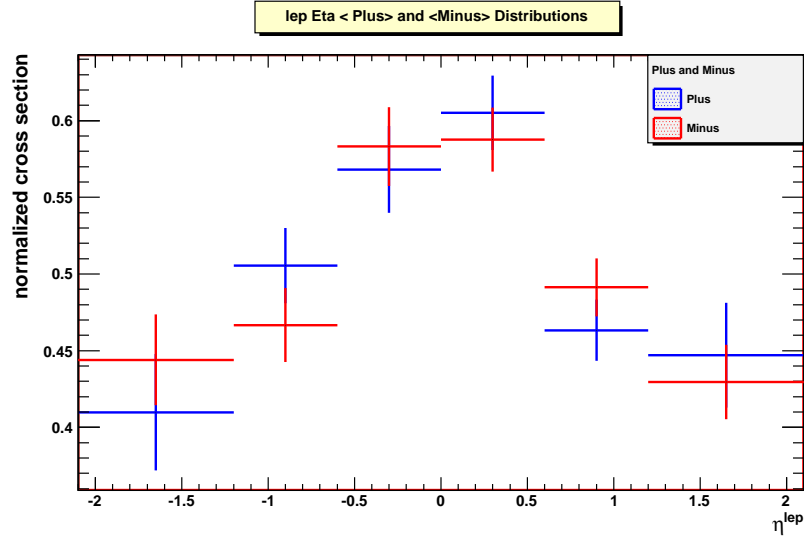


Figure 17: Positively and negatively charged leptons normalized differential cross sections as a function of pseudorapidity η .

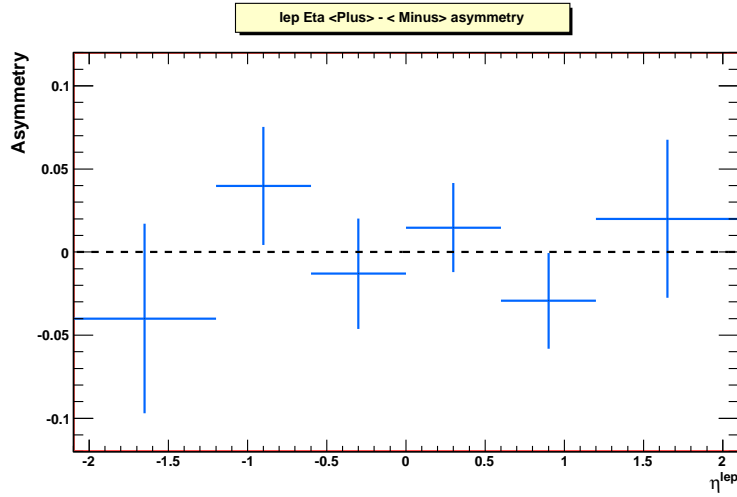


Figure 18: Normalized differential cross section asymmetry for charged leptons as a function of pseudorapidity η .

Both distributions indicate that positively and negatively charged leptons agree within uncertainties regarding their dependence on pseudo-rapidity η . In particular the differential asymmetry is compatible with zero over the full η -range.

3.3.3 Integrated Asymmetry

The results for the integrated lepton charge asymmetries are summarized in Table 2. The lepton charge asymmetry is a tiny effect and even if the resolution in reconstructing lepton quantities is much higher than for jets reconstruction, and hence for top quarks, the present analysis is not yet sensitive enough to measure an integrated asymmetry being significantly different from zero, although the values show a slight trend to small positive values.

Table 2: Integrated charge asymmetries for leptons. The raw asymmetry is obtained from a simulated data sample both for generated and reconstructed events. The cross section asymmetry is measured from a 2011 CMS data set. The uncertainties for the raw asymmetries comprise the statistics only, while the ones for the cross sections contain the statistical and systematic uncertainties.

	Raw asymmetry		Cross section asymmetry	
	Reco Lev	Gen Lev		
η_{lep}	0.98 ± 0.39	0.34 ± 0.12	2.58 ± 1.66	(%)

4 Conclusions

With the present analysis setup two investigations in the framework of semileptonic (electron and muon) top quark pair analysis have been performed based on 5 fb^{-1} of LHC pp-data taken at a center of mass energy of 7 TeV:

1. a comparison of top and antitop quarks regarding their behaviour with respect to transverse momentum and rapidity;
2. a comparison of positively and negatively charged leptons with respect to their dependence on pseudorapidity.

In both cases the raw distributions on generator and reconstruction level as well as normalized differential cross section have been compared. Moreover, differential and integrated asymmetries have been studied.

The main result is that all distributions for both top and antitop quarks as well as for positively and negatively charged leptons agree very well within uncertainties. This furthermore implies that the corresponding asymmetry values are not significantly deviating from zero because the effect turns out to be too small to be measured from distributions directly depending on p_T , y , or η .

A more sensitive definition used by CMS collaboration for $t\bar{t}$ charge asymmetry measurement takes into account the rapidity of top and antitop quarks originating from the same event to evaluate the charge asymmetry [1]. For every top pair the quantity $\Delta|y| = |y_t| - |y_{\bar{t}}|$ is measured and the asymmetry is defined as $A = \frac{N_+ - N_-}{N_+ + N_-}$, where N_+ and N_- are the number of events with $\Delta|y| > 0$ and $\Delta|y| < 0$ respectively. However, it is not possible to follow this “event by event” approach to study lepton charge asymmetries in the semileptonic final state, as the latter characterized by the presence of a single lepton only.

In order to increase the sensitivity of the measurement of the lepton asymmetry and to reduce uncertainties, further improvements could be:

1. extending the η -range to include a larger range of this asymmetry;
2. using an event generator that includes a full NLO implementation. The one used in this analysis (MadGraph) is only approximate NLO meaning that the asymmetry is not entirely implemented, as Figure 7 suggest. This means that the unfolding procedure could bias the result towards a case where the asymmetry is even smaller than expected from nature;
3. repeating the analysis with lepton quantities before the kinematic event reconstruction to profit from the excellent CMS detector resolution and do not smear the kinematics by the fit event reconstruction;
4. performing the analysis in the dilepton decay channel to study other variables like $\Delta|\eta|$ -distributions similarly to the top quark variable $\Delta|y|$ enabling “event by event” analyses.

5 Acknowledgments

I'd like to thank all the Summer Student Programme organizers for their efforts and for making my stay a smooth and pleasurable experience.

I am really thankful to the CMS UniHH Top Quark Group, particularly to Martin, for their pleasant company and for their support during my research project. I am especially grateful to Thomas for introducing me to the world of physics research; it was a very valuable experience to work side by side with him and to benefit from his continuous support and advice.

A final and very special thank you goes to “[basicFunctions.h](#)”, which helped me a lot to improve my knowledge in C++ coding.

6 References

- [1] CMS Collaboration, Measurement of the charge asymmetry in top-quark pair production in proton-proton collisions at $\sqrt{s} = 7TeV$, arXiv:1112.5100v2 [hep-ex] 22 Dec 2011
- [2] CMS Twiki Page <https://twiki.cern.ch/twiki/bin/viewauth/CMS/Web-Home>
- [3] CMS Home Page <http://cms.web.cern.ch>
- [4] https://www.desy.de/h1zeus/combined_results/index.php?do=proton_structure_fits2011_herapdf1.7NLO_figures
- [5] The ROOT team, ”ROOT: An Object Oriented Data Analysis Framework Users Guide 5.26”, <http://root.cern.ch>